☙

Atomically thin hexagonal boron nitride probed by ultrahigh-resolution transmission electron microscopy

Nasim Alem,[1,2] Rolf Erni,[3,4] Christian Kisielowski,[3,4] Marta D. Rossell,[3,4] Will Gannett,[1,3] and A. Zettl[1,2,3,*]

[1]*Department of Physics, University of California at Berkeley, Berkeley, California 94720, USA*
[2]*Center of Integrated Nanomechanical Systems, University of California at Berkeley, Berkeley, California 94720, USA*
[3]*Materials Sciences Division, Lawrence Berkeley National Laboratory, Berkeley, California 94720, USA*
[4]*National Center for Electron Microscopy, Lawrence Berkeley National Laboratory, Berkeley, California 94720, USA*

We present a method to prepare monolayer and multilayer suspended sheets of hexagonal boron nitride (h-BN), using a combination of mechanical exfoliation and reactive ion etching. Ultrahigh-resolution transmission electron microscope imaging is employed to resolve the atoms, and intensity profiles for reconstructed phase images are used to identify the chemical nature (boron or nitrogen) of every atom throughout the sample. Reconstructed phase images are distinctly different for h-BN multilayers of even or odd number. Unusual triangular defects and zigzag and armchair edge reconstructions are uniquely identified and characterized.

I. INTRODUCTION

Boron nitride (BN) is a synthetic material fashionable in both hexagonal and cubic structures.[1–3] Hexagonal BN (h-BN) consists of sp^2-bonded two-dimensional (2D) layers comprising alternate boron and nitrogen atoms in a honeycomb arrangement; these layers are stacked and van der Waals bonded to form a highly anisotropic three-dimensional crystal. The overall structure and atomic spacings of h-BN are very similar to carbon-based graphite.[4,5] In h-BN, however, the boron and nitrogen atoms are alternately stacked directly on top of each other on the adjacent atomic layers resulting in *AAA* stacking (Fig. 1) while graphite maintains an offset Bernal structure (ABA). In addition, the slightly ionic bonding (both in plane and out of plane) in h-BN further sets this material apart from graphite. h-BN is electrically insulating with a large band gap both within and across the layers while graphite is a semimetal with high levels of conductivity within the layers.[1,6,7]

The recent successful isolation and atomic scale investigation of single-layer graphite (i.e., graphene) (Refs. 7–10) has stimulated interest in atomically thin sheets of other layered materials, including BN.[8,11–13] Single layer h-BN is considered the thinnest possible 2D crystal with slightly ionic bonds. This characteristic makes atomically thin h-BN an ideal model system in which to study atomic configurations, including defects, edges, and vacancies of 2D ionic crystals. Of particular interest is the possibility of using an atomic resolution probe to unambiguously identify the atomic species, i.e., to distinguish boron from nitrogen in any particular layer of h-BN. Very recently two independent groups[12,13] have attempted to address this challenge via high-resolution transmission electron microscopy (TEM) of BN modified by *in situ* electron-beam damage. In both studies, suspended atomically thin layers of h-BN were produced using *e*-beam irradiation inside the TEM rather than *ex situ*.

We report here the successful *ex situ* isolation of suspended, single-layer h-BN, achieved using a combination of mechanical exfoliation and reactive ion etching. An ultrahigh-resolution TEM is used to resolve individual atoms

in the lattice and furthermore, the boron and nitrogen atoms are identified using TEM intensity profiles. Higher-layer-number regions of the suspended sample are also investigated along with defect structure and edge configurations. By contrasting atomic intensity profiles for even- and odd-number layers, every atom in the three-dimensional multilayer crystal is identified.

II. SAMPLE PREPARATION AND CHARACTERIZATION

The same mechanical exfoliation methods used to isolate graphene from graphite can also be applied to h-BN.[8,11] However, due to the stronger interplane bonding in h-BN, mononlayer sheets of h-BN are difficult to isolate and at best few atomic-layer specimens are obtained.[11] We have developed an exfoliation and reactive ion etching process that allows suspended, monolayer and higher-number-layer sheets of h-BN to be produced, often with a highly desirable stepwise progression from one layer to higher order layers in a single suspended specimen.

h-BN powder with grade PT 110 was purchased from Momentive Performance Materials and used in this experiment. This material is mechanically cleaved and transferred to the TEM grid as reported by Pacilé *et al.*[11] Boron nitride powder is peeled using adhesive tape and transferred to a silicon wafer with a 300 nm oxide layer. Using optical microscopy, thin BN flakes are identified and transferred to the TEM grid. For this transfer a Quantifoil gold TEM grid from SPI with a perforated carbon film and the hole size of 1.2 μm is placed on top of the BN flake and a drop of isopropanol alcohol is placed on the grid and left to dry. While drying, the carbon film in the TEM grid is pulled down and is adhered to the BN flake as a result of surface tension. Then a drop of polyimide is placed on the TEM grid and the sample is heated at 110 °C for 10 min. After heating, the polyimide is peeled off in one piece, enclosing the TEM grid and the now-adhered BN flake. The sample is placed in a methylpyrrolidone bath for a few hours at 60 °C to dissolve the polyimide. The TEM grid is then transferred to isopropanol solution for a few
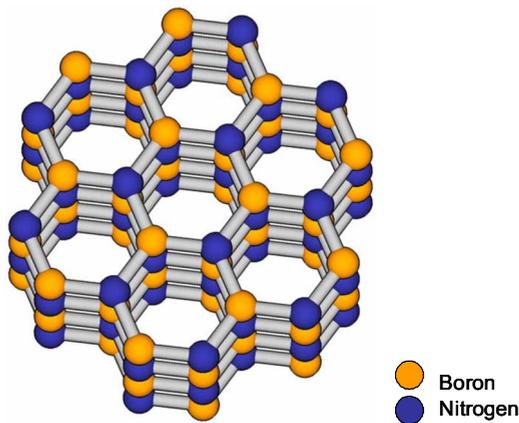
FIG. 1. (Color online) Boron nitride hexagonal lattice. Boron nitride maintains an *AAA* stacking where boron and nitrogen atoms are alternately stacked on top of each other.

minutes and then dried. To further exfoliate the sheet to one monolayer (1 ML), the reactive ion etching technique is used. The exfoliation was performed on the TEM sample in a Plasma Etch model PE-200. In this study, we used a mixture of oxygen and nitrogen plasmas with the energy varying between 22 and 30 W to further exfoliate the BN TEM samples down to a monolayer.

An ideal tool with which to characterize atomic structure, defects, and edges in thin free-standing membranes is a high-resolution TEM. Conventional TEMs, however, do not have the required resolution for distinguishing atoms in h-BN and are often operated at very high voltages leading to immediate sample damage before any reliable observations can be made. To avoid these issues, we utilize the TEAM 0.5, an ultrahigh-resolution aberration-corrected TEM that operates at 80 kV. This microscope provides sub-Angstrom resolution at 80 kV and is thus capable of imaging individual atoms in the h-BN lattice with minimal structural damage.[14,15]

The TEAM 0.5 microscope is equipped with an imaging aberration corrector and a source electron monochromator. The monochromator was setup to obtain an energy spread of the electron beam of less than 0.2 eV (full width at half maximum). Considering the constant of chromatic aberration of 1.1 mm at 80 kV, the energy spread of the beam results in a focus spread of $\sim$1.2 nm (rms) and an information limit of $\sim$0.08 nm. Phase contrast transmission electron microscopy was carried out at 80 kV with the third-order spherical aberration C_3 set to -18 μm. Single lattice images were recorded at a defocus of about +10 nm. The settings for C_3 and defocus optimize the imaging conditions according to Lentzen[17] taking into account the finite fifth-order spherical aberration C_5 that comes at the expense of minimizing off-axial coma. Off-axial coma of third order B_3 is a geometrical aberration which causes off-axial object points to be imaged as trailing patterns. Since B_3 affects off-axial image points, it essentially violates the isoplanatic approximation. In order to approach an isoplanatic information transfer, radial off-axial coma B_3 needs to be minimized such that the amount of equally resolved image points is a maximum. However, minimizing off-axial coma leads to a finite value of C_5 which in our case was 7 mm.[16] This imaging condition, optimized according to Lentzen,[17] results in atoms appearing bright on a dark background. Through-focal series were recorded
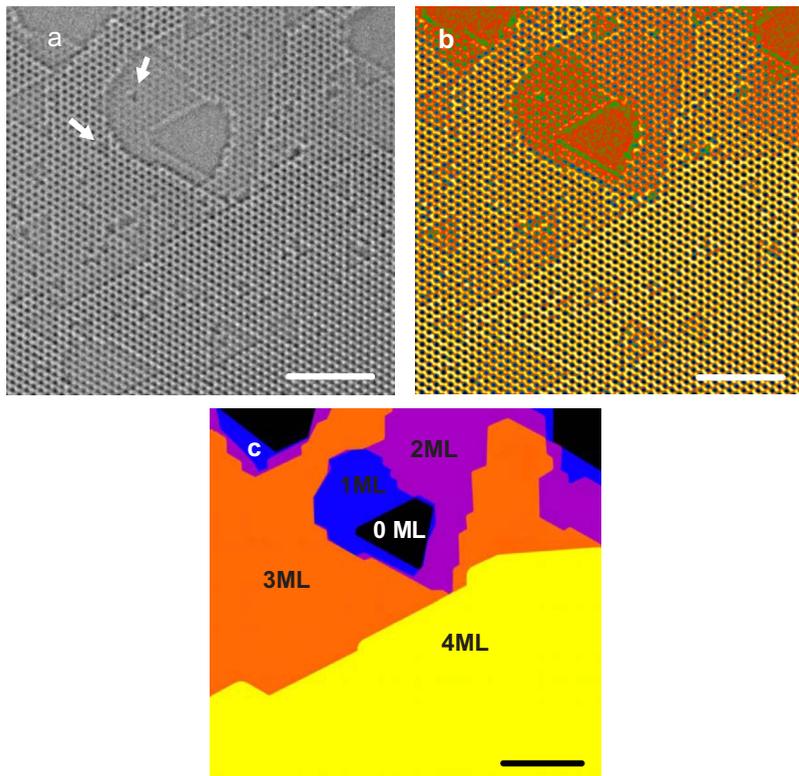
FIG. 2. (Color online) Atomic structure of a one- to four-layer BN with its thickness map. (a) High resolution TEM image of BN. (b) The color gradient BN reconstructed phase image shown in (a). (c) A thickness map indicating the number of layers in boron nitride imaged here. The scale bar is 2 nm in this figure.

within a focal range of +12 to −12 nm employing a focal step of 0.6 nm.

Multislice simulations were carried out using the MacTempas software employing a set of parameters in agreement with the experimental conditions. We calculated the complex electron wave at the exit plane of the specimen in order to have a direct comparison with the exit plane wave restored from through focal series. The figure of merit is the phase shift of the exit-plane wave.

III. RESULTS AND DISCUSSION

Figure 2(a) shows a high-resolution TEM image of a suspended thin h-BN specimen. The most striking features of the image are a small-scale periodicity and larger-scale intensity variations, including intensity variations with triangular symmetry. The small-scale periodic bright spots correspond to individual B or N atoms (or atomic columns) in the expected honeycomb arrangement, with a nearest-neighbor in-plane B-N distance of 1.4 Å, in agreement with the known crystal structure of h-BN.[18] The larger-scale intensity variations in Fig. 2(a) correspond to differences in layer number across the specimen, including the regions of missing atoms. In addition, the triangular intensities, marked on Fig. 2(a), represent the point defects formed in BN. As we demonstrate below, we are able to identify every atom in every layer in the specimen within the TEM field of view.

A. Layer number identification

In order to identify the number of atomic layers in a given region of the suspended specimen, we use a reconstructed phase image of one- to four-layer BN previously shown in Fig. 2(a). From the reconstructed phase image [Fig. 2(b)] we extract a general layer number or thickness map for the entire specimen within the TEM field of view. We are aided by knowledge that for multilayers (i.e., regions with layer number $n > 1$), the atoms in normal projection for *AAA* stacking are located directly on top of one another (see Fig. 1). Our simulations show that, under the assumption that the specimen is thinner than the focal spread, the intensity at an atomic position increases approximately linearly with each additional layer (B and N have very similar scattering power). Thus, from the intensity profiles in Fig. 2(b) (and ignoring for the moment the regions of localized defects), we obtain the layer number thickness map of Fig. 2(c), where each color represents the general extent of a given total thickness, from 1 ML thick up to four layers thick (4 ML). The three black regions, labeled 0 ML, correspond to holes in the membrane (i.e., vacuum). Figure 2(c) shows examples of where the sample thickness increases in unity monolayer steps; however, there are also locations where an edge step corresponds to an abrupt jump by two or more layers. Such distinctions will prove to be particularly important in the atom identification analysis below.

B. Atom identification

Boron and nitrogen have similar atomic numbers and core electron configurations, hence similar scattering power for TEM imaging electrons. The resulting intensity profiles for individual B and N atoms in the reconstructed phase image for a monolayer region are thus expected to be similar but not identical. In a Previous TEM study of h-BN, Meyer *et al.*[12] were unable to unambiguously distinguish boron from nitrogen. To distinguish B from N requires the necessary resolution *and* sensitivity (signal to noise). To improve signal to noise, we sum 20 images of the BN unit cell randomly selected from a defect-free monolayer region of the h-BN specimen (see Fig. 2). The normalized unit-cell image and its standard deviation thus obtained are shown in the upper left part of Fig. 3(a). Similar results are obtained for two-, three-, and four-layer regions and are also shown in Fig. 3(a). The donut-shaped rings around the atom positions in the standard deviation plots reflect thermal- and electron-beam-induced bond vibrations in the BN lattice.

Figure 3(b) presents line profiles through the unit-cell intensity data of Fig. 3(a), for $n=1$ through $n=4$. The two peaks in each line scan represent adjacent columns of atoms linking the h-BN layers. For the monolayer ($n=1$), a slight but distinct asymmetry in the peak heights is observed. This asymmetry largely disappears for $n=2$ and 4 but reappears for $n=3$. We thus find asymmetry only for columns of atoms with an odd number of atoms (i.e., layers). Figure 3(c) shows schematically an edge-on profile view of the atomic structure of successive BN monolayers built up stepwise. With imaging electrons impinging from above and probing columns of atoms, only columns within an odd number of layers may have differences in the total number of atoms of one species. Columns within an even number of layers always have $n/2$ boron atoms and $n/2$ nitrogen atoms.

We have simulated the scattering of electron beam for the parameters appropriate to our microscope and sample, with results shown in Fig. 3(d). Within experimentally relevant limits, we find from these simulations that for $n=1–4$ the intensity for a column of atoms depends only on the total number of B atoms and the total number of N atoms, not on the order of such atoms in the column. The simulations show a clear intensity asymmetry for adjacent columns in the odd-layer-number regions, $n=1$ and 3, and no discernible asymmetry for adjacent columns in even-layer-number regions, $n=2$ and 4. Nitrogen yields the stronger intensity in this representation. Hence, for the experimental data of Fig. 3(b), we identify the smaller peak in the monolayer line scan as belonging to B and the larger peak as belonging to N. Once B and N are identified within a unit cell in the monolayer (B or N as the majority atom in an odd-layer-number region), all other atoms in the h-BN crystal specimen are uniquely chemically identified, as can be readily inferred from Fig. 3(c).

It is worth noting potential TEM instrumentation errors that can easily lead to erroneous image intensity results and the misidentification of the atomic sublattices in thin h-BN specimens. One error is sample tilt, where the TEM imaging electron beam is not perfectly normal to the sample layers. Another is axial coma B_2 of second order which can arise from a miscentered optical element that produces third-order spherical aberration C_3, i.e., the objective lens of positive C_3 and/or the aberration corrector with negative C_3. The axial coma B_2 is a geometrical aberration which affects all image
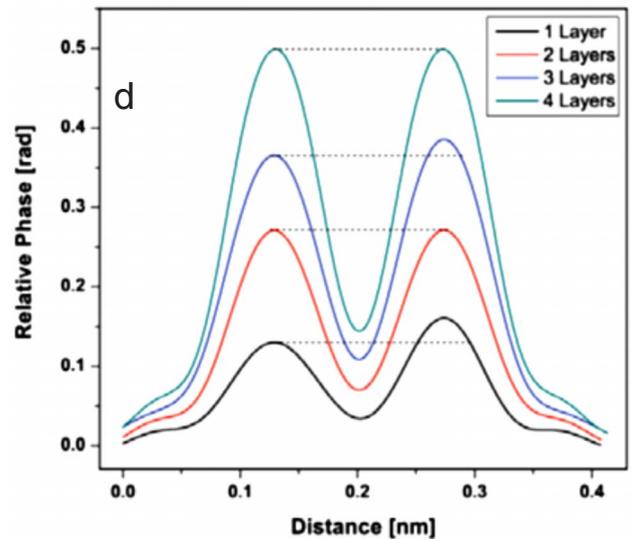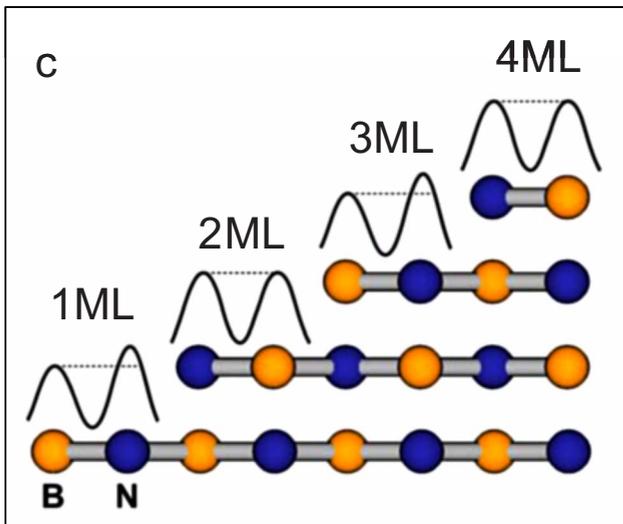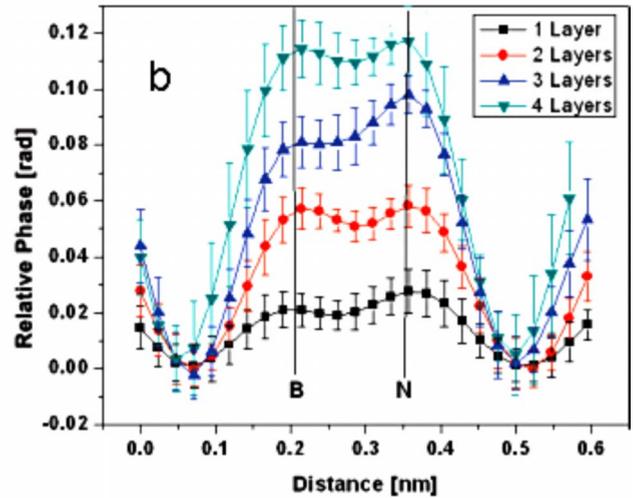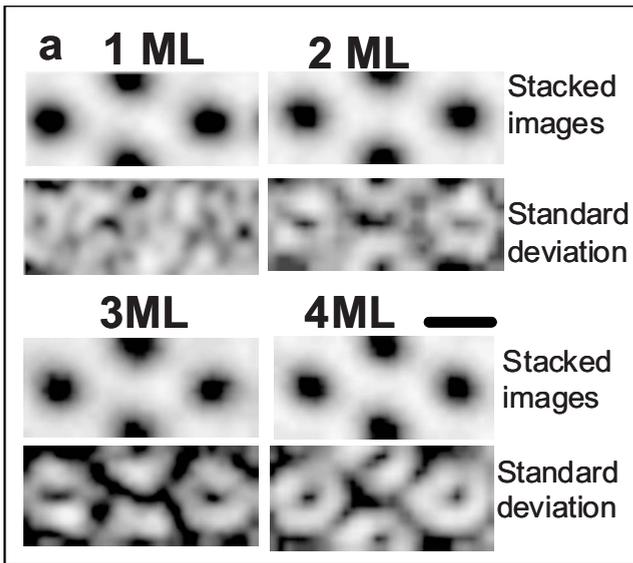
FIG. 3. (Color online) The image of the sum of 20 unit cells in a one- to four-layer BN and its intensity line profile. (a) The resulting images from the summation of 20 unit cells in a one- to four-layer BN. The scale bar shows 1.5 Å. (b) The intensity line profile from the unit-cell images previously shown in (a). (c) A model for the edge-on structure of BN lattice with its mean atomic projected potential (shown on top of the lattice). (d) The simulated intensity modulations in an exit wave phase image for a single- to four-layer area in BN.

points equally independent from their distance to the optical axis. Axial coma thus causes all object points to be imaged as trailing patterns which show a distinct coma halo. Axial coma thus isoplanatically breaks the isotropic symmetry of the information transfer. With suitable deflectors axial coma B_2 can be minimized. However, a small finite effect of residual B_2 can still occur and impact the information transfer. In cases where this problem exist, we have found both experimentally and through detailed simulations that spurious intensity line scan asymmetries can appear between adjacent atomic columns, uncorrelated with the actual projected chemical potential of the atom (see the supplementary section in Ref. 29). Indeed, with such problems present, the apparent asymmetries often increase with increasing layer number (including even-layer numbers), rather than falling

to zero for even number layers as shown correctly in Figs. 3(b) and 3(d). In a recent TEM study on the identification of boron and nitrogen in atomically thin h-BN, Jin *et al.*[13] used intensity profiles in the reconstructed phase image to distinguish B from N. However, their adjacent atom (column) asymmetry for an identified $n=2$ bilayer exceeds their asymmetry plotted for an identified $n=1$ monolayer. This is in contradiction to the experimental results and simulations presented here, where the asymmetry disappears in even-layer-number regions of h-BN. According to our investigations, particular care must be taken to eliminate residual aberrations, slight mistilt, and axial coma, all of which can significantly distort contrast asymmetry in h-BN and compromise atom identification. Such distortions have also been observed and noted by Meyer *et al.*[12]
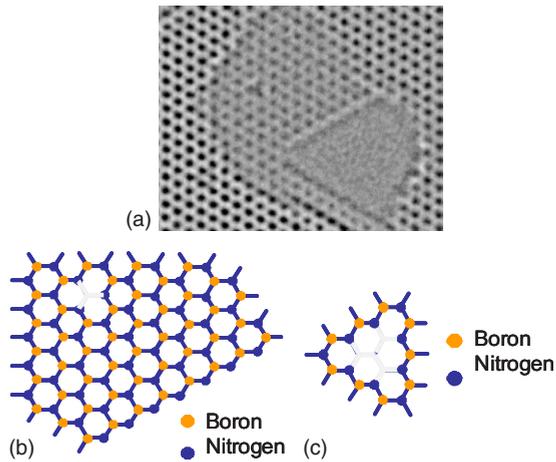
FIG. 4. (Color online) Lattice structure in a monolayer of BN. (a) Reconstructed phase image of BN with a triangular monovacancy and a large vacancy previously pointed to by arrows in Fig. 2(a). (b) A model indicating the position of boron and nitrogen atoms in the monolayer BN. This model shows the monovacancy to form as a result of a boron atom missing and the edges to be nitrogen terminating zigzag edges. (c) A model showing the boron and nitrogen atom positions in the large vacancy at the lower left side in (a). The scale bar is 1 nm.

FIG. 5. (Color online) HRTEM image of BN sheet at the edge. BN sheets show both (a) zigzag and (b) armchair edges. The scale bar is 1 nm.

Unambiguous identification of the sublattices in h-BN sets the stage for proper interpretation of defect structure. Figure 2(a) shows a host of unusual crystal imperfections. The plethora of defects observed in this figure is most likely not a good representation of the original "as-grown" h-BN specimen but is a consequence of the rather severe reactive ion etching process used to thin the sample. In addition, we have observed that the electron beam itself creates vacancies through knock-on damage.

The two arrows in Fig. 2(a) point to defects resulting from missing atoms within a layer. Figure 4(a) shows the same defects in a magnified, reconstructed phase image. The upper defect resides in an $n=1$, monolayer region of the sample, while the lower defect resides in an $n=3$ region. We create a model for the atom positions in the monolayer by repeating the previously identified BN unit cell for this layer. Figure 4(b) shows the model positions of boron and nitrogen atoms in the monolayer region. According to this figure the monovacancy is a missing B atom. We find that monovacancies throughout the sample appear to be predominantly associated with missing boron atoms. Preferential formation of boron monovacancies in the sample under the 80 keV electrons is expected since the energy threshold for the knock-on damage of boron and nitrogen atoms in h-BN is 74 eV and 84 keV, respectively, assuming an otherwise perfect monolayer crystal.[19]

Besides boron monovacancies just described, we observe larger triangle-shaped vacancies, which result from clusters of multiple missing atoms. Numerous such defects are observable in Fig. 2(a), with different sizes and orientations. We consider the lower triangular defect identified with an arrow in Fig. 2(a) [and again in Fig. 4(a)] which resides in a three-layer region. Since all atoms in this $n=3$ region have been previously identified by the methods presented above,
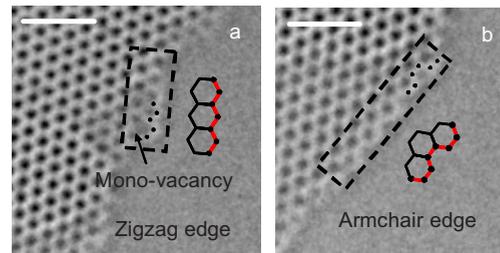
we unambiguously find that this large vacancy results from three missing boron atoms and one nitrogen atom, most likely grouped together on either the top or the bottom layer (momentum transfer from electron knock-on effects would suggest the missing atoms are from the bottom layer). Figure 4(c) shows a model of the defect and indicates that the "internal" edges of this vacancy maintain a nitrogen-terminated zigzag configuration. These observations are in agreement with the previously identified defects in h-BN.[12,13,20]

We examine the edge configurations for large-scale layer terminations, including holes in the monolayer and atomic step edges. As just discussed, nitrogen-terminated zigzag edges are stable for trianglelike defects. Beside defect edges, this edge configuration is also observed by the holes in monolayer and multilayer regions [Fig. 5(a)]. Alternating B-N armchair edges also exist in BN [Fig. 5(b)], albeit with far less frequency than N-terminated zigzag edges. In this study we have observed that zigzag edges in BN are more stable under the TEM electron beam. A recent study on the edge dynamics in a single-layer graphene has shown that the single- or double-bonded carbon atoms at the edges are less stable under the electron beam and therefore have a lower knock-on energy threshold.[21–24] Similar to graphene, we believe the higher stability of the nitrogen-terminated zigzag edges in h-BN are most likely related to the difference in knock-on energy threshold for B versus N (even at the edge), together with an intrinsic preference for zigzag configurations generally in planar sp^2-bonded sheet materials.

The successful isolation of free-standing monolayer membranes of h-BN by a straightforward exfoliation/reactive ion etching method has made possible sequential-monolayer ultrahigh-resolution TEM studies of this material. The honeycomb in-plane structure and anisotropic bonding between layers allows comparison to graphene and graphite while the presence of two atomic sublattices and consequent ionic character of the bonding in h-BN dictates different interlayer stacking and markedly different defect structure from the carbon analogs. The successful distinction of boron from nitrogen within an h-BN monolayer and the identification of the B and N sublattices throughout the entire crystal is an important advance for 2D crystal investigations. Although graphene and h-BN have similar atomic structures, we find no evidence for the formation of Stone-Wales-type defects in BN sheets, presumably due to unfavorably high formation energy of B-B and N-N bonds in the BN lattice (a similar argument applies for BN nanotubes).[25,26]

Atomic vibrations around monovacancies, edges, and within the lattice in h-BN layers, have been explored. The

standard deviation images in Fig. 3(a) show the extent of such motion and the white rings surrounding the atom positions quantify these excursions. Such vibrations are more significant in a monolayer since the atoms are only confined in a two-dimensional space, not by extra bonds at the top and the bottom. In the three- and four-layer areas, in contrast, the atoms experience ionic forces applied to them from the top and the bottom layers. Bond relaxations and distortions also occur in the vicinity of monovacancies and edges. Our TEM observations show that the bond vibrations can lead to the distortion of the vacancy which can further break its three-fold symmetry. Such distortions can be related to hybridization of sp^2 orbitals of the edge atoms at the vicinity of the vacancy and the Jahn-Teller effect.[27,28] Further studies are warranted for bond distortions induced by adsorption of adatoms, such as hydrogen, to the sheet atoms and to the dangling bonds at the edge of the vacancy in particular.

IV. CONCLUSIONS

We report on a method to exfoliate atomically thin BN sheets using the reactive ion etching technique. This exfoliation technique can be applied to similar materials to create atomically thin two-dimensional sheets at large size scales.

In addition, the atom identification technique employed here to differentiate boron from nitrogen in BN can be applied to identify the atomic species and consequently the nature of defects and edges in other similar low-dimensional crystals. Single layer boron nitride is the thinnest ionic material that can exist in two dimensions. Similar to graphene, this material offers a unique model system to study the stability and dynamics of defects, edges and vacancies, and their interactions with the adatoms in ionic crystals.

ACKNOWLEDGMENTS

*Author to whom correspondence should be addressed. azettl@berkeley.edu

[1] K. Watanabe, T. Taniguchi, and H. Kanda, Nature Mater. **3**, 404 (2004).

[2] T. Taniguchi, K. Watanabe, and S. Koizumi, Phys. Status Solidi A **201**, 2573 (2004).

[3] V. A. Gubanov, Z. W. Lu, B. M. Klein, and C. Y. Fong, Phys. Rev. B **53**, 4377 (1996).

[4] A. Rubio, J. L. Corkill, and M. L. Cohen, Phys. Rev. B **49**, 5081 (1994).

[5] N. G. Chopra, R. J. Luyken, K. Cherrey, V. H. Crespi, M. L. Cohen, S. G. Louie, and A. Zettl, Science **269**, 966 (1995).

[6] K. S. Novoselov, A. K. Geim, S. V. Morozov, D. Jiang, M. I. Katsnelson, I. V. Grigorieva, S. V. Dubonos, and A. A. Firsov, Nature (London) **438**, 197 (2005).

[7] K. S. Novoselov, A. K. Geim, S. V. Morozov, D. Jiang, Y. Zhang, S. V. Dubonos, I. V. Grigorieva, and A. A. Firsov, Science **306**, 666 (2004).

[8] K. S. Novoselov, D. Jiang, F. Schedin, T. J. Booth, V. V. Khotkevich, S. V. Morozov, and A. K. Geim, Proc. Natl. Acad. Sci. U.S.A. **102**, 10451 (2005).

[9] J. C. Meyer, A. K. Geim, M. I. Katsnelson, K. S. Novoselov, D. Obergfell, S. Roth, C. Girit, and A. Zettl, Solid State Commun. **143**, 101 (2007).

[10] J. C. Meyer, A. K. Geim, M. I. Katsnelson, K. S. Novoselov, T. J. Booth, and S. Roth, Nature (London) **446**, 60 (2007).

[11] D. Pacilé, J. C. Meyer, Ç. Ö. Girit, and A. Zettl, Appl. Phys. Lett. **92**, 133107 (2008).

[12] J. C. Meyer, A. Chuvilin, G. Algara-Siller, J. Biskupek, and U. Kaiser, Nano Lett. **9**, 2683 (2009)

[13] C. Jin, F. Lin, K. Suenaga, and S. Iijima, Phys. Rev. Lett. **102**, 195505 (2009).

[14] C. Kisielowski, B. Freitag, M. Bischoff, H. Van Lin, S. Lazar, G. Knippels, P. Tiemeijer, P. M. van der Stam, S. von Harrach, M. Stekelenburg, M. Haider, S. Uhlemann, H. Muller, P. Hartel, B. Kabius, D. Miller, I. Petrov, E. A. Olson, T. Donchev, E. A. Kenik, A. R. Lupini, J. Bentley, S. J. Pennycook, I. M. Anderson, A. M. Minor, A. K. Schmid, T. Duden, V. Radmilovic, Q. M. Ramasse, M. Watanabe, R. Erni, E. A. Stach, P. Denes, and P. U. Dahmen, Microsc. Microanal. **14**, 469 (2008).

[15] J. C. Meyer, C. Kisielowski, R. Erni, M. D. Rossell, M. F. Crommie, and A. Zettl, Nano Lett. **8**, 3582 (2008).

[16] H. Müller, S. Uhlemann, P. Hartel, and M. Haider, Phys. Procedia **1**, 167 (2008).

[17] M. Lentzen, Microsc. Microanal. **14**, 16 (2008).

[18] B. G. Demczyk, J. Cumings, A. Zettl, and R. O. Ritchie, Appl. Phys. Lett. **78**, 2772 (2001).

[19] A. Zobelli, A. Gloter, C. P. Ewels, G. Seifert, and C. Colliex, Phys. Rev. B **75**, 245402 (2007).

[20] W. Auwarter, M. Muntwiler, J. Osterwalder, and T. Greber, Surf. Sci. **545**, L735 (2003).

[21] Ç. Ö. Girit, J. C. Meyer, R. Erni, M. D. Rossell, C. Kisielowski, L. Yang, C. H. Park, M. F. Crommie, M. L. Cohen, S. G. Louie, and A. Zettl, Science **323**, 1705 (2009).

[22] R. F. Egerton, F. Wang, and P. A. Crozier, Microsc. Microanal. **12**, 65 (2006).

[23] B. W. Smith and D. E. Luzzi, J. Appl. Phys. **90**, 3509 (2001).

[24] V. H. Crespi, N. G. Chopra, M. L. Cohen, A. Zettl, and S. G. Louie, Phys. Rev. B **54**, 5927 (1996).

[25] X. Blase, A. De Vita, J.-C. Charlier, and R. Car, Phys. Rev. Lett. **80**, 1666 (1998).

[26] A. Loiseau, F. Willaime, N. Demoncy, G. Hug, and H. Pascard,

Phys. Rev. Lett. **76**, 4737 (1996).

[27] S. Azevedo, J. R. Kaschny, C. M. C. De Castilho, and F. D. Mota, Eur. Phys. J. B **67**, 507 (2009).

[28] R. F. Liu and C. Cheng, Phys. Rev. B **76**, 014405 (2007).

[29] See EPAPS Document No. E-PRBMDO-80-091935 for our other article on this subject entitled, "The effect of mistilt and coma during HRTEM imaging." For more information on EPAPS, see http://www.aip.org/pubservs/epaps.html